Synthesis of Cadmium Selenide Quantum Dots from a Non-Coordinating Solvent: Growth Kinetics and Particle Size Distribution

ARTICLE *in* THE JOURNAL OF PHYSICAL CHEMISTRY C · OCTOBER 2008

Impact Factor: 4.77 · DOI: 10.1021/jp803746b

4 AUTHORS, INCLUDING:

Kwan Hyi Lee
Korea Institute of Science and Technology
39 PUBLICATIONS **306** CITATIONS
SEE PROFILE

Justin F Galloway
Johns Hopkins University
7 PUBLICATIONS **115** CITATIONS
SEE PROFILE

Peter Searson
Johns Hopkins University
297 PUBLICATIONS **11,770** CITATIONS
SEE PROFILE

Article

Synthesis of Cadmium Selenide Quantum Dots from a Non-Coordinating Solvent: Growth Kinetics and Particle Size Distribution

Jeaho Park, Kwan Hyi Lee, Justin F. Galloway, and Peter C. Searson

J. Phys. Chem. C, **2008**, 112 (46), 17849-17854 • DOI: 10.1021/jp803746b • Publication Date (Web): 29 October 2008

Synthesis of Cadmium Selenide Quantum Dots from a Non-Coordinating Solvent: Growth Kinetics and Particle Size Distribution

Jeaho Park, Kwan Hyi Lee, Justin F. Galloway, and Peter C. Searson*,†

Department of Materials Science and Engineering, Johns Hopkins University, Baltimore, Maryland 21218

Received: April 29, 2008; Revised Manuscript Received: June 19, 2008

Here we report on the synthesis of CdSe quantum dots from a noncoordinating solvent. We show that nucleation and growth is very fast and is completed within 100 s. The subsequent increase in average particle size is due to diffusion limited coarsening. Growth and coarsening can be quenched by injection of dodecanethiol. Finally, we compare the size distribution obtained from analysis of the absorption edge with the size distribution obtained from analysis of transmission electron microscope images.

Introduction

Semiconductor quantum dots (QDs) have received considerable attention due to their size dependent properties and applications in fields such as solar cells,[1] light emitting diodes,[2] and biological imaging.[3,4] For materials, such as quantum dots, that exhibit size dependent properties, it is essential to understand the details of nucleation and growth and how they influence the evolution of the particle size and the particle size distribution.

CdSe is one of the most versatile quantum dot materials since its emission wavelength can be tuned across the visible spectrum. CdSe has a band gap of about 1.72 eV[5] corresponding to a band-to-band emission wavelength of about 730 nm. As the particle diameter decreases below about 10 nm, band gap enlargement becomes significant and blue emission can be achieved for particles about 3 nm in diameter.

The most common synthesis route for CdSe QDs involves an organometallic precursor in a coordinating solvent.[6−8] Typically dimethyl cadmium is reacted with selenium in trioctylphosphine oxide at elevated temperature, usually about 300 °C. The addition of more strongly co-ordinating molecules, can lead to anisotropic growth and the synthesis of quantum rods.[9−11] More recently, high quality CdSe QDs have been synthesized from "greener" precursors such as CdO and Cd acetate, thereby avoiding many of the limitations associated with the organometallic precursor.[8,12−14] The CdO precursor is reacted with Se in TOP, with the addition of another coordinating ligand, such as hexadecylamine, or a phosphonic acid.

The CdSe QDs studied here are synthesized from a noncoordinating solvent, octadecene, with oleic acid as a capping ligand. The reaction can be performed very simply by injecting the precursor mixture into the solvent with the capping ligand at 290 °C. This is similar to the method reported for the synthesis of InP, InAs, and CdS QDs.[15,16] We show that nucleation and growth are fast and that the subsequent increase in particle size is due to diffusion limited coarsening. Finally, we show that growth can be quenched by injection of dodecanethiol. We also show that the particle size distribution obtained from analysis of the absorption edge is in good agreement with the distribution obtained from analysis of transmission electron microscope images.

Experimental Details

Synthesis. First, 0.1 M solutions of the cadmium (Cd) and selenium (Se) precursors were prepared separately. The Cd precursor was prepared by mixing 0.3204 g CdO (Alfa Aesar, Puratronic, 99.998%), 6.94 mL oleic acid (OA, Aldrich, Technical grade 90%), and 18 mL 1-octadecene (ODE, Aldrich, tech. 90%) at 220 °C until the solution became transparent. The Se precursor was prepared by dissolving 0.1579 g Se powder (Aldrich, 100mesh 99.5+ %) in 20 mL trioctylphosphine (TOP, Aldrich, Technical grade 90%) with sonication for at least 190 min in a glovebox. One mL of each precursor was combined while sonicating to make 2 mL of the Cd/Se precursor.

Next, 9 mL of ODE and 1 mL of OA were combined in a 3-neck flask and heated to 100 − 120 °C while stirring vigorously under vacuum for 5 − 10 min. The temperature was then increased to 290 °C under inert gas (Ar) flow, with cold water running through the condenser. The Cd/Se precursor (2 mL) was then rapidly injected into the hot solution. We note that the temperature for this synthesis is easily achieved using a heating mantle and does not require additional insulation.

Small aliquots (typically about 1 mL) were extracted from the mixture at different reaction times. The extracted aliquots were immediately immersed in dry ice in order to quench further growth of the nanocrystals. One mL of hexane (EMD, HPLC grade) was added to each aliquot. Next, 2 mL methanol (EMD, HPLC grade) was added into the solution for washing. When the separation between two layers was evident, the clear bottom layer was discarded; this washing procedure was repeated three times. After washing the remaining organics and solvent, acetone was added until the solution became opaque. The supernatant was discarded after centrifugation at 8000 rpm for 10 min. The solid precipitate was redissolved in about 1 mL hexane.

Capping. For capping experiments, 8 mL 1-dodecanethiol (Aldrich, ≥98%) was injected into the QD suspensions resulting in a final concentration of 1.65 M. The addition of 0.033 mol dodecanethiol corresponds to an excess of 1193 with respect to monolayer coverage on 5.8 nm diameter particles assuming that all precursor is reacted to form CdSe and all of the surfactant is adsorbed on the particles. The concentration of the CdSe QDs is 0.1 mmol (3.22×10^{16} CdSe particles) under this assumption

* To whom correspondence should be addressed. E-mail: searson@jhu.edu.

† Institute for NanoBioTechnology, Johns Hopkins University, Baltimore, Maryland 21218.

10.1021/jp803746b CCC: $40.75
Published on Web 10/29/2008

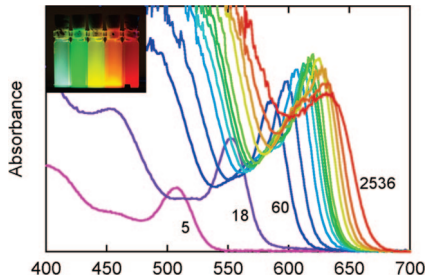

Figure 1. Absorbance spectra for CdSe QDs after reaction times from 5 to 2536 s. The inset shows a photograph of suspensions of CdSe QDs after 2, 10, 30, 120, 480 s under UV excitation.

with a total CdSe surface area of 3.403×10^{18} nm^2. Assuming an adsorption area of 20 Å^2 for the thiols, then monolayer coverage corresponds to 0.028 mmol dodecanethiol (6.8 μL dodecanethiol).

Characterization. Photoluminescence measurements were obtained using a fluorometer (Fluorolog-3 fluorometer, Horiba Jobin Yvon). Absorbance spectra of the samples were obtained using a spectrophotometer (Cary 50 UV/vis). Suspensions of the CdSe QDs in hexane were placed in cuvettes with polished sides (Starna Cells, Inc.). Transmission electron microscope images were obtained with a Philips EM 420 TEM and FEI Tecnai 12 TWIN. High resolution images were obtained using a Philips CM 300 FEG TEM. Samples for transmission electron microscopy were prepared by placing a drop of the QD suspension on a lacey-carbon grid.

The quantum yield (QY) was determined using Rhodamine 6G as a standard. Rhodamine 6G has a QY of 95% at an excitation wavelength of 488 nm.[17] The calibration curve for Rhodamine was obtained in DI water which has refractive index (n_{st}) of 1.333. The integrated area under the fluorescence curves (excitation at 488 nm) was plotted versus the absorbance at 488 nm (after subtraction of the solvent absorbance) for different concentrations. The same procedure was repeated for the QD samples suspended in hexane ($n = 1.3749$). The excitation intensity and slit width were held constant for all measurements. The QY of the QDs was obtained from $QY_{QD} = QY_{st}\,[(dI/dA)_{QD}/(dI/dA)_{st}]\,[n_{QD}^2/n_{st}^2]$ where I is the area under the PL curves and A is the corresponding absorbance.[18]

Results and Discussions

Particle Synthesis. Figure 1 shows a sequence of absorbance spectra as a function of reaction time after injection of the Cd/Se precursor mixture. The absorbance spectra show an exciton peak close to the absorption onset, characteristic of many semiconductor quantum dots. The overall absorbance at short wavelengths (<420 nm) increases with time, saturating after about 100 s. The absorption edge is relatively sharp, indicating a relatively narrow size distribution.[19] With increasing reaction time, the absorbance spectra red shift indicating a progressive increase in the average particle size.

Particle sizes were determined from analysis of TEM images. Figure 2 shows typical TEM images for CdSe QDs prepared at different reaction times. In all cases the particles appeared spherical and relatively monodisperse. Figure 2a shows an image of particles synthesized for 180 s where the average radius is 3.3 nm. Large areas of the grid revealed particles self-assembled into ordered close packed arrays, although no attempt was made to optimize conditions for self-assembly. The inset in Figure 2a shows a high resolution TEM image of a single QD where the lattice fringes show that the particle is a single crystal.

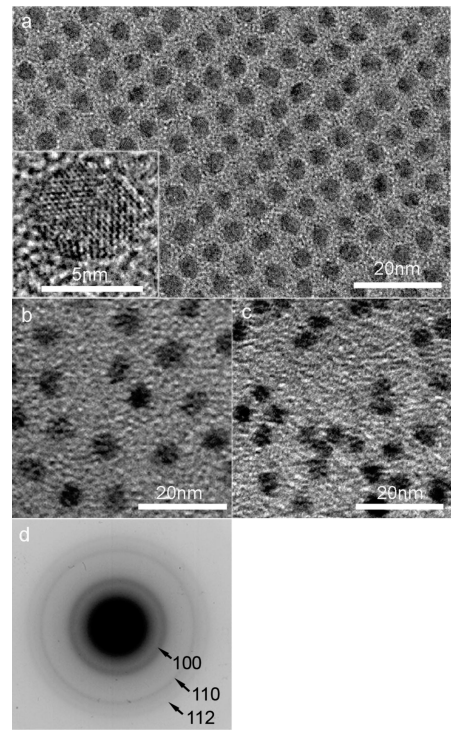

Figure 2. TEM images of CdSe QDs. Reaction time (a) 180, (b) 60, (c) 10 s. Average particle size (radius) (a) 3.3, (b) 3.2, (c) 2.5 nm. The inset shows a high resolution TEM image of a CdSe after 180 s. (d) The selected area electron diffraction pattern confirms the wurtzite crystal structure.

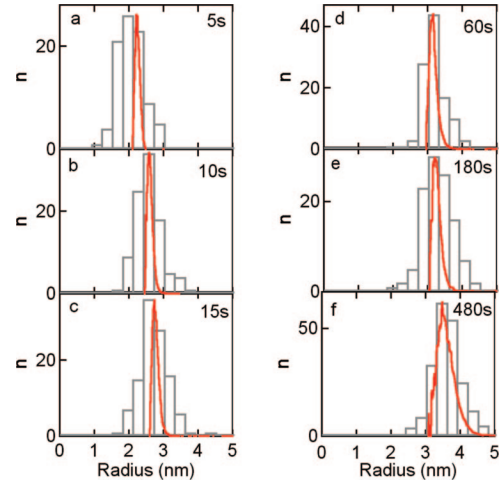

Figure 3. Size distribution histograms obtained from TEM images. Reaction time: (a) 5 ($N = 88$), (b) 10 ($N = 110$), (c) 15 ($N = 97$), (d) 60 ($N = 106$), (e) 180 ($N = 111$), (f) 480 s ($N = 205$). (Solid lines) Size distributions calculated from absorbance spectra based.

Figures 2b and 2c show particles after 60 and 10 s reaction time. The selected area electron diffraction pattern (Figure 2d) confirms that wurtzite crystal structure.

The size distributions of the particles, obtained from analysis of the TEM images are shown in Figure 3. The distributions appear symmetrical and the most-probable radius increases from 2.5 nm at 5 s to 3.6 nm after 480 s. The size distributions are relatively sharp even though no size selection was performed in the synthesis.

Figure 4 shows PL spectra for a series of CdSe QDs with reaction times from 2 to 480 s, corresponding at average particle radii of 2.0−3.6 nm. For all experiments with this reaction scheme, spectra obtained for reaction times less than 5 s

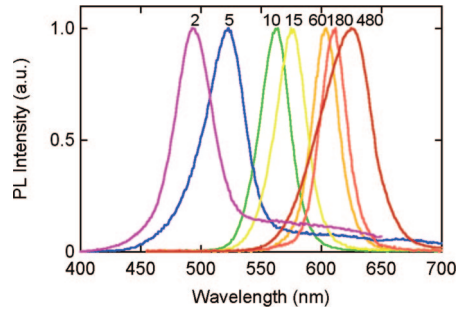

Figure 4. Photoluminescence spectra of CdSe QDs. The reaction time in seconds is indicated in the figure.

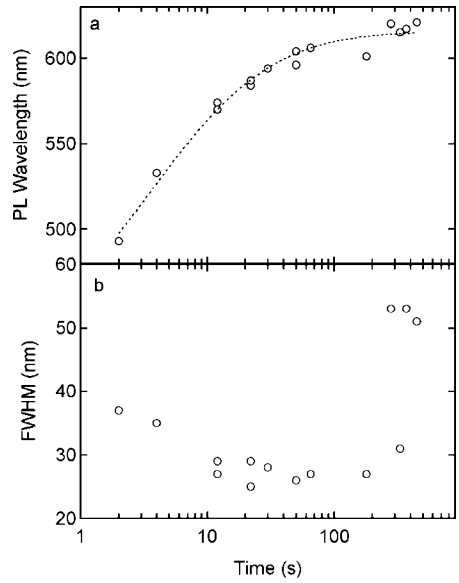

Figure 5. (a) PL peak wavelength and (b) fwhm versus the logarithm of the reaction time.

exhibited a small shoulder at longer wavelengths, whereas the spectra at longer times were symmetrical. The PL peak and full width at half-maximum (fwhm) are shown in Figure 5. The PL peak red shifts significantly in the first 50 s and then increases more slowly at longer times. The fwhm decreases slightly over the first 200 s and then increases sharply at longer times. For reaction times from 20 to 200 s, the fwhm is less than 30 nm, equivalent to the best results reported using other synthesis methods.[6,13,14,20] The quantum yield for the QDs decreased slightly from 11.5% ($t = 15$ s) to 7.8% ($t = 200$ s). These values are in good agreement with reports in the literature for uncapped CdSe QDs.[7,21]

An estimate of the average particle diameter can be obtained from the PL peak. Assuming that the PL is due to band-to-band emission, then the wavelength at the PL peak can be used to obtain the band gap. The average particle size can then be estimated from the band gap using a suitable model for confinement.[22] Figure 6 shows the band gap for CdSe QDs versus particle radius compared to the effective mass model. In the effective mass model the band gap is related to the particle size by[23]

$$E^* = E_g^{bulk} + \frac{\hbar^2\pi^2}{2er^2}\left(\frac{1}{m_e m_o} + \frac{1}{m_h m_o}\right) - \frac{1.8e}{4\pi\varepsilon\varepsilon_o r} \qquad (1)$$

where E^* is the band gap in eV, E_g^{bulk} is the bulk band gap, r is the particle radius, m_e is the effective mass of the electrons, m_h is the effective mass of the holes, m_o is the mass of a free electron, ε is the relative permittivity, ε_o is the permittivity of

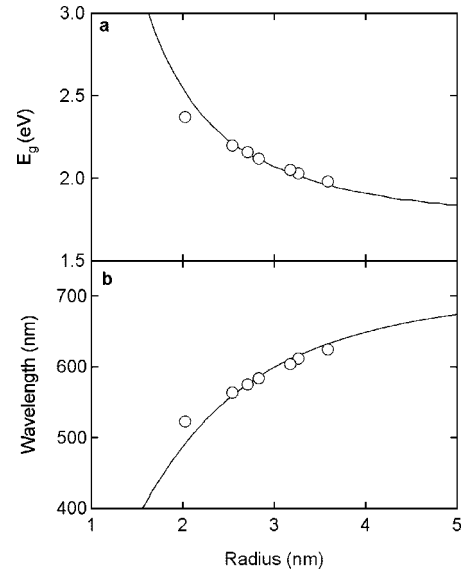

Figure 6. (a) Average band gap obtained from analysis of TEM images and (b) corresponding wavelength plotted versus average particle radius. The solid line corresponds to the effective mass model using E_g(bulk) = 1.72 eV, $m_e = 0.13$ and $m_h = 0.45$, and $\varepsilon = 10$.

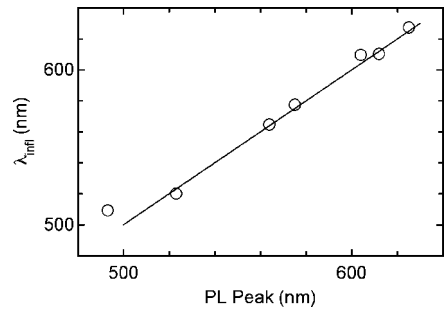

Figure 7. Plot of the PL peak wavelength (Figure 5a) versus the wavelength at the inflection point in the absorbance edge of the absorbance spectra (Figure 1).

free space, $\hbar$ is Planck's constant, and e is the charge on the electron. The second term on the right is a quantum confinement term and the third term is an electrostatic attraction between the electron and hole. For CdSe we take $E_g^{bulk} = 1.72$ eV, $m_e = 0.13$, $m_h = 0.45$, and $\varepsilon = 10$.[5]

From Figure 6 we see that there is good agreement between the average particle size obtained from analysis of TEM images and the effective mass model down to a radius of about 2 nm, corresponding to an emission wavelength of 520 nm. We did not analyze TEM images for smaller particles due to the difficulty in obtaining precise measurements on a sufficiently large number of particles. Murray et al.[6] reported good agreement between the average size of CdSe QDs obtained from analysis of TEM images and the effective mass model, but only for particle radii down to about 3 nm. For smaller particles, the band gap enlargement was smaller than predicted by the model. Nonetheless, this correlation provides a convenient tool for estimating the average particle diameter from PL spectra without the need for direct measurement using transmission electron microscopy, at least for radii from 2 to 4 nm.

An estimate of the average diameter of QDs in suspension can also be obtained from absorbance spectra. Figure 7 shows that the wavelength at the inflection point in the absorbance edge (i.e., the point where $d^2A/d\lambda^2 = 0$) is in excellent agreement with the wavelength of the PL peak, illustrating that the same particle size would be obtained from absorbance or PL spectra.

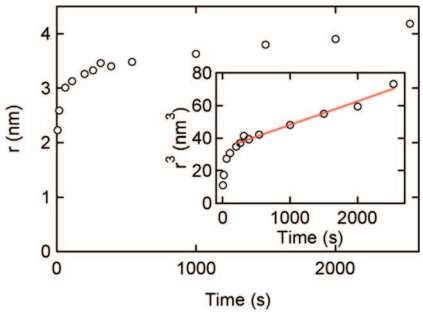

Figure 8. Particle radius versus reaction time. The particle size was obtained from the inflection point in absorbance spectra using the effective mass model. The inset shows a plot of r^3 versus time.

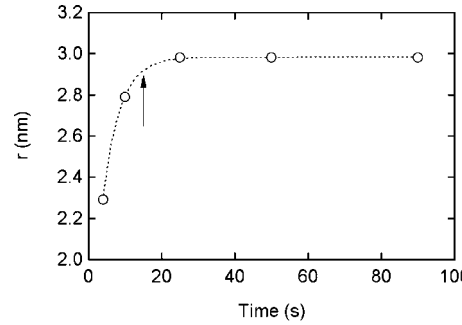

Figure 9. Particle radius versus reaction time. At 15 s, dodecanethiol was injected into the reaction mixture.

The time dependence of the average particle size obtained from absorbance spectra has been used to study the kinetics of growth and coarsening of QDs during synthesis.[24−26]

Growth and Coarsening. During synthesis, the Cd and Se precursors combine to form stable nuclei that subsequently grow as the reaction proceeds. The synthesis reported here is a simple one-pot synthesis where the precursor mixture is injected into the solvent/capping ligand solution at the reaction temperature for reaction times up to 2500 s. For the short reaction times, QDs that emit in the blue are easily obtained. At longer times, particle growth results in a progressive red shift, resulting in larger particles that emit in the red, approaching the emission wavelength of 730 nm for band-to-band emission from bulk CdSe. These results are consistent with previous reports using dimethyl cadmium precursor, a co-ordinating solvent, and more complex thermal management schemes.[7]

The increase in particle size with reaction time during solution phase synthesis involves nucleation, growth, and other processes such as aggregation and coarsening. Bullen and Mulvaney have shown that nucleation of CdSe from octadecene is very fast and stops almost immediately after precursor injection.[27] Examination of the absorption spectra from several experiments reveals that the absorbance at short wavelengths reaches a maximum very quickly, within the first 100 s. For an inorganic semiconductor, the absorbance at short wavelengths is related to the total volume of the material and hence this result indicates that the precursor concentration has decreased to the saturation concentration and that growth is completed within 100 s.

Subsequent changes in particle size can, therefore, only occur by processes such as coarsening or aggregation. Figure 8 shows a plot of particle radius versus time for a typical CdSe synthesis. The average particle radius was obtained from the inflection point in the absorption edge using the effective mass model, as described above. The particle radius increases very quickly in the first 50 s, after which the particle size increases much more slowly. The inset shows the particle radius replotted as r^3 versus time. The linear region from about 200 s until 2500 s is consistent with diffusion limited coarsening which has a rate law given by $r_{av}^3 - r_0^3 = kt$.[28,29]

From the slope of the linear region we obtain the rate constant for coarsening $k = 0.010 \pm 0.0047$ nm^3 s^{-1} ($N = 6$). This is somewhat larger than the rate constant for coarsening of ZnO in alcohol which in the range $10^{-4}-10^{-3}$ nm^3 s^{-1}, depending on anion, solvent, and temperature (25 − 65 °C).[30−33] The rate constant is given by[31−33]

$$k = \frac{8\gamma V_m^2 c_{r=\infty}}{54\pi\eta a N_A} \qquad (2)$$

where γ is the surface energy, V_m is the molar volume, $c_{r=\infty}$ is the equilibrium concentration at a flat surface (i.e., the bulk solubility), η is the viscosity of the solvent, a is the solvated ion radius, and N_A is Avogadro's number. Since γ, V_m, η, and a are known or can be reasonably estimated, we can obtain an estimate for the bulk solubility of CdSe in octadecene at 290 °C. The surface energy of solids at a solid−liquid interface is expected to be in the range 0.1−0.5 J m^{-2},[34] and a value of 0.17 J m^{-2} has been reported for CdSe QDs in octadecene.[27] The molar volume V_m for CdSe at 300 K is 32.9 cm^3 mol^{-1} and since the linear expansion coefficient is about 7.4×10^{-6} K^{-1}, [35] we take the same value for V_m at the reaction temperature. Since octadecene is a noncoordinating solvent, we use the ionic radius $a = 0.1$ nm for the solvated ion radius.[36] The viscosity of octadecene at 290 °C is estimated by extrapolation from lower temperatures (using $\ln \eta = -4.986 + 1879/T$),[37] giving a value of 0.19 cP. Taking $k = 0.01$, we estimate a bulk solubility of 0.02 nM for CdSe in the reaction mixture. This value is about 8 orders of magnitude lower than the precursor concentration (8.33 mM), providing a broad window for particle growth and confirming that most of the precursor reacts to form the solid phase. The bulk solubility is also within the range 0.01−1 nM, estimated for ZnO during synthesis in alcohol.[31,32]

These results reveal two important features of CdSe synthesis. First, nucleation and growth is very fast and is completed within the first 100 s. Second, the subsequent increase in average particle size is due to diffusion limited coarsening. Figure 5a shows that the PL peak red shifts significantly in the first 50 s, corresponding to the nucleation and growth phase. After 50 s, the rate at which the PL peak red shifts decreases significantly in the regime where coarsening controls the increase in particle size. The fwhm of the PL peak decreases slightly during the first 100 s and then increases sharply to about 50 nm after several hundred seconds (Figure 5b).

The importance of coarsening in QDs transferred to clean solvent after synthesis has been highlighted by experiments where CdSe QDs synthesized from hexadecylamine were transferred to toluene.[38] Both CdSe and CdSe/ZnSe QDs showed an increase in the average particle size due to diffusion limited coarsening for times up to 8 h after transferring to the clean solvent.

Coarsening requires thermodynamic equilibrium at the particle surface between the solid and liquid phases, indicating that the oleic acid and trioctylphosphine are weakly physisorbed to the surface. Figure 9 shows the particle radius plotted versus time for CdSe synthesis where an excess of dodecanethiol were injected after 15 s. The particle radius does not increase after injection showing that the thiol is chemisorbed to the surface and thereby preventing coarsening. Octadecanethiol has been shown to quench growth during synthesis of ZnO.[39]

Particle Size Distributions. For a bulk semiconductor, the shape of the absorption edge is determined by the electronic

band-to-band transition.[40] For an ensemble of QDs, the shape of the absorption edge close to the absorbance onset, is also dependent on the particle size distribution and hence the distribution of band gaps. However, if the particle size distribution is sufficiently large, then the shape of the absorbance spectrum near the absorbance onset is dominated by the particle size distribution. Thus the particle size distribution can be obtained from analysis of the absorption edge.

For sufficiently dilute suspensions, the absorbance A at any wavelength in the quantum regime is related to the total volume of particles with radius greater than or equal to the size corresponding to the absorption onset[19]

$$A(r) \propto \int_r^\infty \frac{4}{3}\pi r^3 n(r) dr \quad (3)$$

where $n(r)$ is the particle size distribution. The particle size distribution can be obtained from the absorbance edge by taking the derivative of $A(r)$ with respect to the particle radius, and noting that as $r \rightarrow \infty$, $n(r) = 0$:

$$n(r) \propto -\frac{dA(r)/dr}{\frac{4}{3}\pi r^3} \quad (4)$$

Having established that the effective mass model can be used to relate the band gap to the particle radius (Figure 6), we can determine the particle size distribution from the absorption edge. As described above, the particle size distribution is simply related to the local slope of the absorbance spectrum at the absorption edge. The procedure is as follows. First the absorption edge is extracted from the absorption spectrum. This is the region from the absorption onset to the point where the slope is zero (the exciton peak). Next the wavelength axis is converted to energy and then to radius using the effective mass model. A suitable fitting method is used to obtain the slope ($dA(r)/dr$) at each radius. Finally, $dA(r)/dr$) is divided by the particle volume at that radius to obtain $n(r)$.

The particle size distributions obtained from analysis of the absorption edges are superimposed on the distributions obtained from analysis of the TEM images in Figure 3. There is excellent agreement between the most probable size obtained from analysis of the absorption edge and the TEM images, as expected from Figure 6. The maximum in the distribution obtained from analysis of the absorbance spectra corresponds to the inflection point in the absorption edge and can be considered the average particle size.

The particle size distribution obtained from the absorbance spectra at 480 s ($r_{av} = 3.6$ nm) shows good agreement with the distribution obtained from analysis of TEM images. For shorter reaction times, the distributions obtained from analysis of the absorbance spectra are progressively sharper than the distributions obtained from TEM images. This may be the result of the difficulty in obtaining precise measurements of smaller particles from TEM images. It is also evident that the distributions obtained from the absorbance spectra are noticeably sharper to the left of the maximum at small particle sizes. This effect is likely due to the contribution of the exciton peak and can be seen from the absorbance spectra in Figure 1. We note, however, that particles in this size regime comprise only a small volume fraction of the overall distribution and we make no attempt to subtract the contribution of the exciton peak from the absorbance spectra.

These measurements show that a reasonable estimate of the particle size distribution for CdSe QDs can be obtained from analysis of the absorbance spectra, without the necessity of transmission electron microscopy.

Summary

We report on the synthesis of CdSe QDs using a noncoordinating solvent at 290 °C. QDs with PL emission from blue to red can be easily obtained with a narrow full width at half-maximum. Nucleation and growth are fast and completed within the first 100 s. The subsequent slow increase in average particle size is due to diffusion limited coarsening. Growth and coarsening can be quenched by injection of dodecanethiol. We show that the average particle size and PL peak agree very well with the effective mass model at least for radii from 2 to 4 nm. This relationship has been used to compare the particle size distribution from analysis of the absorption edge and the distribution obtained from transmission electron microscopy.

Acknowledgment. We gratefully acknowledge Dr. M. McCaffrey and Dr. K. Livi for assistance with TEM imaging. We also acknowledge Dr. M. Merzlyakov for assistance with PL measurements. J.P. acknowledges a Summer Fellowship from the Johns Hopkins Institute of NanoBioTechnology. This work was supported by NIH (1R21EB006890-01).

References and Notes

(1) Huynh, W. U.; Peng, X. G.; Alivisatos, A. P. *Adv. Mater.* **1999**, *11*, 923–927.
(2) Mattoussi, H.; Radzilowski, L. H.; Dabbousi, B. O.; Thomas, E. L.; Bawendi, M. G.; Rubner, M. F. *J. Appl. Phys.* **1998**, *83*, 7965–7974.
(3) Gao, X. H.; Cui, Y. Y.; Levenson, R. M.; Chung, L. W. K.; Nie, S. M. *Nat. Biotechnol.* **2004**, *22*, 969–976.
(4) Michalet, X.; Pinaud, F. F.; Bentolila, L. A.; Tsay, J. M.; Doose, S.; Li, J. J.; Sundaresan, G.; Wu, A. M.; Gambhir, S. S.; Weiss, S. *Science* **2005**, *307*, 538–544.
(5) Berger, L. I. *Semiconductor materials*; CRC Press: Boca Raton, FL, 1997.
(6) Murray, C. B.; Norris, D. J.; Bawendi, M. G. *J. Am. Chem. Soc.* **1993**, *115*, 8706–8715.
(7) Dabbousi, B. O.; RodriguezViejo, J.; Mikulec, F. V.; Heine, J. R.; Mattoussi, H.; Ober, R.; Jensen, K. F.; Bawendi, M. G. *J. Phys. Chem. B* **1997**, *101*, 9463–9475.
(8) Peng, Z. A.; Peng, X. G. *J. Am. Chem. Soc.* **2001**, *123*, 183–184.
(9) Peng, Z. A.; Peng, X. G. *J. Am. Chem. Soc.* **2001**, *123*, 1389–1395.
(10) Peng, X. G.; Manna, L.; Yang, W. D.; Wickham, J.; Scher, E.; Kadavanich, A.; Alivisatos, A. P. *Nature* **2000**, *404*, 59–61.
(11) Yu, H.; Li, J. B.; Loomis, R. A.; Gibbons, P. C.; Wang, L. W.; Buhro, W. E. *J. Am. Chem. Soc.* **2003**, *125*, 16168–16169.
(12) Qu, L. H.; Peng, Z. A.; Peng, X. G. *Nano Lett.* **2001**, *1*, 333–337.
(13) Qu, L. H.; Peng, X. G. *J. Am. Chem. Soc.* **2002**, *124*, 2049–2055.
(14) Mekis, I.; Talapin, D. V.; Kornowski, A.; Haase, M.; Weller, H. *J. Phys. Chem. B* **2003**, *107*, 7454–7462.
(15) Battaglia, D.; Peng, X. G. *Nano Lett.* **2002**, *2*, 1027–1030.
(16) Yu, W. W.; Peng, X. G. *Angew. Chem., Int. Ed.* **2002**, *41*, 2368–2371.
(17) Magde, D.; Rojas, G. E.; Seybold, P. G. *Photochem. Photobiol.* **1999**, *70*, 737–744.
(18) Demas, J. N.; Crosby, G. A. *J. Phys. Chem.* **1971**, *75*, 991–1024.
(19) Pesika, N. S.; Stebe, K. J.; Searson, P. C. *J. Phys. Chem. B* **2003**, *107*, 10412–10415.
(20) Talapin, D. V.; Rogach, A. L.; Kornowski, A.; Haase, M.; Weller, H. *Nano Lett.* **2001**, *1*, 207–211.
(21) Murray, C. B.; Kagan, C. R.; Bawendi, M. G. *Science* **1995**, *270*, 1335–1338.
(22) Efros, A. L.; Rosen, M. *Annu. Rev. Mater. Sci.* **2000**, *30*, 475–521.
(23) Brus, L. *J. Phys. Chem.* **1986**, *90*, 2555–2560.
(24) Bahnemann, D. W.; Kormann, C.; Hoffmann, M. R. *J. Phys. Chem.* **1987**, *91*, 3789–3798.
(25) Wong, E. M.; Bonevich, J. E.; Searson, P. C. *J. Phys. Chem. B* **1998**, *102*, 7770–7775.
(26) van Dijken, A.; Meulenkamp, E. A.; Vanmaekelbergh, D.; Meijerink, A. *J. Phys. Chem. B* **2000**, *104*, 1715–1723.
(27) Bullen, C. R.; Mulvaney, P. *Nano Letters* **2004**, *4*, 2303–2307.

(28) Lifshitz, I. M.; Slyozov, V. V. *J. Phys. Chem. Solids* **1961**, *19*, 35–50.
(29) Wagner, C. *Z. Elektrochem.* **1961**, *65*, 581–591.
(30) Hu, Z. S.; Ramirez, D. J. E.; Cervera, B. E. H.; Oskam, G.; Searson, P. C. *J. Phys. Chem. B* **2005**, *109*, 11209–11214.
(31) Hu, Z. S.; Oskam, G.; Penn, R. L.; Pesika, N.; Searson, P. C. *J. Phys. Chem. B* **2003**, *107*, 3124–3130.
(32) Hu, Z. S.; Oskam, G.; Searson, P. C. *J. Colloid Interface Sci.* **2003**, *263*, 454–460.
(33) Hu, Z. S.; Santos, J. F. H.; Oskam, G.; Searson, P. C. *J. Colloid Interface Sci.* **2005**, *288*, 313–316.
(34) Zangwill, A. *Physics at surfaces*; Cambridge University Press: Cambridge, 1988.
(35) Kumar, V.; Sastry, B. S. R. *Cryst. Res. Technol.* **2001**, *36*, 565–569.
(36) Shannon, R. D. *Acta Crystallogr., Sect. A* **1976**, *32*, 751–767.
(37) Kang, J. W.; Yoo, K. P.; Kim, H. Y.; Lee, H.; Yang, D. R.; Lee, C. S. *Int. J. Thermophys.* **2001**, *22*, 487–494.
(38) Sung, Y. M.; Park, K. S.; Lee, Y. J.; Kim, T. G. *J. Phys. Chem. C* **2007**, *111*, 1239–1242.
(39) Wong, E. M.; Hoertz, P. G.; Liang, C. J.; Shi, B. M.; Meyer, G. J.; Searson, P. C. *Langmuir* **2001**, *17*, 8362–8367.
(40) Pankove, J. I. *Optical processes in semiconductors*; Dover: New York, 1975.

JP803746B